Steady-state Saturated Groundwater Flow Modeling with Full Tensor Conductivities Using Finite Differences

Liangping Li*, **Haiyan Zhou**, **J. Jaime Gómez-Hernández**

Group of Hydrogeology, Universidad Politécnica de Valencia, Spain

Abstract

We present a new three-dimensional steady-state saturated groundwater-flow forward-simulator with full conductivity tensors using a nineteen-points block-centered finite-difference method. Hydraulic conductivity tensors are defined at the block interfaces eliminating the need to average conductivity tensors at adjacent blocks to approximate their values at the interfaces. The capabilities of the code are demonstrated in three heterogeneous formulations, two of the examples are two-dimensional, and the third one is three-dimensional and uses a nonuniform discretization grid. A benchmark, in the context of conductivity upscaling, is carried out with the MODFLOW LVDA module, which uses hydraulic conductivity tensors at block centers and then approximates their values at the interfaces. The results show that our code gives more accurate predictions for the interblock fluxes than the MODFLOW LVDA module when the block conductivity principal directions are not parallel to the Cartesian axis.

Key words: Full tensor; Upscaling; Finite difference; Interblock; Flow simulation

1. Introduction

One of the major problems faced by hydrologists is how to deal with the spatial variability of hydraulic conductivities. In the early stages of numerical groundwater flow modeling, it was common to assume very mild heterogeneities, limited to a layer-cake description of the aquifer and some zonation of conductivities within each layer. Then, for the solution, a standard seven-point block-centered finite-difference approach is, even today, typically employed to solve the partial differential equation in three dimensions. This formulation assumes an alignment of the block sides and principal directions (Harbaugh et al., 2000) of hydraulic conductivity, and uses the arithmetic mean (upper bound, Penman (1988)) or the harmonic mean (lower bound, Duvaut et al. (1976)) of neighboring block conductivities to approximate their values at block interfaces. (Recall that the finite-difference formulation of groundwater flow uses the conductivities at the interfaces as equation parameters). However, these approaches have two shortcomings: first, they assume that the block conductivity is, at most, a diagonal tensor, that is, it could be anisotropic to flow but always with its principal directions parallel to the Cartesian axes; and second, they generally assume that the harmonic mean is the value that best approximate the conductivities at the interface. Both assumptions are flawed when we consider that the numerical model is always a simplification of a very heterogeneous spatial distribution of hydraulic conductivities at a scale much smaller than that of the discretization. For one thing, the spatial heterogeneity within the numerical block could seldom be upscaled to a diagonal tensor, in general the tensor would be non-diagonal, particularly in environments in which cross-bedding is observed (Bierkens and Weerts, 1994), or where heterogeneity is high; for another, even acknowledging that the exact approximate for the equivalent conductivity of two homogeneous blocks with flow across their interface is

*Corresponding author

Email addresses: liali@upvnet.upv.es (Liangping Li), haizh@upvnet.upv.es (Haiyan Zhou), jaime@dihma.upv.es (J. Jaime Gómez-Hernández)

their harmonic mean, this is not the best approximation when we consider that each block value is already some upscaled value of a set of the underlying heterogeneous conductivities; in such a case, the best upscaled value for the interface could be a different average value, moreover, if the block conductivities are tensors, it is not clear how to average two tensors.

Cross-bedding (Bierkens and Weerts, 1994), blocks the size of which is about the correlation length of the underlying conductivity (Wen and Gómez-Hernández, 1996), or the misalignment between stratification and computational grid (Bear, 1972) are some of the causes that would require an analysis with full conductivity tensors, or, in other words, that would imply that the flow direction may not be parallel to the piezometric head gradient.

Several authors have approached the problem of groundwater flow simulation with non-null off-diagonal components in the conductivity tensor. Aavatsmark et al. (1996) derived a method that is proposed for control volume formulations on quadrilateral grids in two dimensions. Continuity conditions at the interfaces are enforced to construct the discretization method for non-orthogonal curvilinear grids. Edwards and Rogers (1998) developed a general theory for curvilinear coordinates but present a full set of coefficients for only the homogeneous case. Later, Anderman et al. (2002) extended this method for the heterogeneous case, and incorporated it in MODFLOW in two dimensions, namely in the package layer variable-direction horizontal anisotropy capacity (LVDA). An alternative is to use finite elements, or better control-volume finite-element methods (Rozon, 1989), however, the finite element formulation will always introduce unwanted discontinuities at control-volume boundaries (Aavatsmark et al., 1996).

In this context, we present a nineteen-point block-centered finite-difference scheme, which solves the steady-state groundwater flow equation with full tensor conductivities in three dimensions on a nonuniform grid. Because finite difference formulations use the conductivity values at block interfaces, the program takes as input values the interface conductivity tensors directly, i.e., it will not approximate them from block values. This approach is particularly suitable when the numerical model is a coarse model derived from a fine scale heterogeneous model through upscaling (Zhou et al., 2010).

Our objectives in this paper are: (1) to present a new forward simulator with full conductivity tensors; (2) to compare its performance with the LVDA package in MODFLOW; (3) to describe how to treat Dirichlet and Neumann boundary conditions with irregularly shaped boundaries; (4) to demonstrate the capabilities of the code in three dimensions with a non-uniform grid.

The outline of this paper is as follows. We first introduce the flow governing equation and discuss the simulation algorithm. Next, the flowchart of the algorithm is illustrated with an emphasis on the numerical implementation. Then, the capabilities of the proposed approach are demonstrated using two types of heterogeneous formations, in the context of upscaling, making use of the upscaling code written by Zhou et al. (2010) and presented in an accompanying paper. Finally, numerical tests for nonuniform blocks in three dimensions are shown to demonstrate the accuracy and efficiency of the proposed simulator.

2. Flow Simulator Algorithm

The steady-state groundwater flow equation of an incompressible or slightly compressible fluid in saturated porous media in a Cartesian coordinate system can be expressed as:

$$\nabla \cdot (\mathbf{K} \nabla h) + q = 0, \tag{1}$$

where $h = h(\mathbf{x}, t)$ is the piezometric head $[L]$; $q = q(\mathbf{x}, t)$ is the volumetric source flow per unit volume $[T^{-1}]$; $\nabla\cdot = (\frac{\partial}{\partial x} + \frac{\partial}{\partial y} + \frac{\partial}{\partial z})$ is the divergence operator of a vector field; and $\nabla = (\frac{\partial}{\partial x}, \frac{\partial}{\partial y}, \frac{\partial}{\partial z})^T$ is the gradient operator of a scalar field.

In its most general formulation, the hydraulic-conductivity tensor $\mathbf{K} = \mathbf{K}(\mathbf{x})$ is a symmetric full tensor of rank three and has the form:

$$\mathbf{K} = \begin{bmatrix} K_{xx} & K_{xy} & K_{xz} \\ K_{xy} & K_{yy} & K_{yz} \\ K_{xz} & K_{yz} & K_{zz} \end{bmatrix}. \tag{2}$$

The partial differential equation governing steady-state groundwater flow in three dimensions can be rewritten as,

$$\begin{aligned}&\frac{\partial}{\partial x}\Big(K_{xx}\frac{\partial h}{\partial x}+K_{xy}\frac{\partial h}{\partial y}+K_{xz}\frac{\partial h}{\partial z}\Big)+\frac{\partial}{\partial y}\Big(K_{xy}\frac{\partial h}{\partial x}+K_{yy}\frac{\partial h}{\partial y}+K_{yz}\frac{\partial h}{\partial z}\Big)+\\&\frac{\partial}{\partial z}\Big(K_{xz}\frac{\partial h}{\partial x}+K_{yz}\frac{\partial h}{\partial y}+K_{zz}\frac{\partial h}{\partial z}\Big)+q=0.\end{aligned}\tag{3}$$

If this equation is discretized with a nineteen-point block-centered finite-difference scheme with nonuniform parallel-piped blocks, the following equation results(see Figure 1),

$$\begin{aligned}&\frac{1}{\Delta x|_{i,j,k}}\left[\Big(K_{xx}\frac{\partial h}{\partial x}+K_{xy}\frac{\partial h}{\partial y}+K_{xz}\frac{\partial h}{\partial z}\Big)\Big|_{i+1/2,j,k}-\Big(K_{xx}\frac{\partial h}{\partial x}+K_{xy}\frac{\partial h}{\partial y}+K_{xz}\frac{\partial h}{\partial z}\Big)\Big|_{i-1/2,j,k}\right]+\\&\frac{1}{\Delta y|_{i,j,k}}\left[\Big(K_{xy}\frac{\partial h}{\partial x}+K_{yy}\frac{\partial h}{\partial y}+K_{yz}\frac{\partial h}{\partial z}\Big)\Big|_{i,j+1/2,k}-\Big(K_{xy}\frac{\partial h}{\partial x}+K_{yy}\frac{\partial h}{\partial y}+K_{yz}\frac{\partial h}{\partial z}\Big)\Big|_{i,j-1/2,k}\right]+\\&\frac{1}{\Delta z|_{i,j,k}}\left[\Big(K_{xz}\frac{\partial h}{\partial x}+K_{yz}\frac{\partial h}{\partial y}+K_{zz}\frac{\partial h}{\partial z}\Big)\Big|_{i,j,k+1/2}-\Big(K_{xz}\frac{\partial h}{\partial x}+K_{yz}\frac{\partial h}{\partial y}+K_{zz}\frac{\partial h}{\partial z}\Big)\Big|_{i,j,k-1/2}\right]+\\&q_{i,j,k}=0,\end{aligned}\tag{4}$$

for a block (i,j,k) of size $\Delta x|_{i,j,k}\times\Delta y|_{i,j,k}\times\Delta z|_{i,j,k}$.

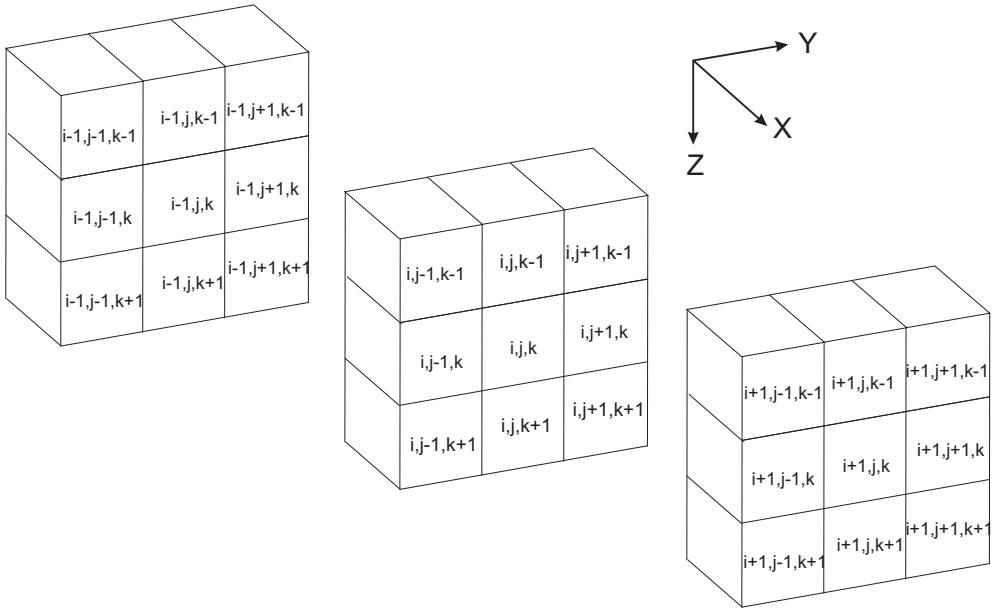

Figure 1: Schematic illustration of the three dimensional finite difference spatial discretization

The hydraulic gradients at the interfaces are approximated by central differences from the heads at the nineteen blocks surrounding (i,j,k), That is,

$$
\begin{aligned}
\left.\frac{\partial h}{\partial x}\right|_{i+1/2,j,k} &= \frac{h_{i,j+1,k} - h_{i,j-1,k}}{\triangle x|_{i,j+1,k} + 2\triangle x|_{i,j,k} + \triangle x|_{i,j-1,k}} + \frac{h_{i+1,j+1,k} - h_{i+1,j-1,k}}{\triangle x|_{i+1,j+1,k} + 2\triangle x|_{i+1,j,k} + \triangle x|_{i+1,j-1,k}} \\
\left.\frac{\partial h}{\partial y}\right|_{i+1/2,j,k} &= \frac{2(h_{i+1,j,k} - h_{i,j,k})}{\triangle y|_{i+1,j,k} + \triangle y|_{i,j,k}} \\
\left.\frac{\partial h}{\partial z}\right|_{i+1/2,j,k} &= \frac{h_{i,j,k+1} - h_{i,j,k-1}}{\triangle z|_{i,j,k+1} + 2\triangle z|_{i,j,k} + \triangle z|_{i,j,k-1}} + \frac{h_{i+1,j,k+1} - h_{i+1,j,k-1}}{\triangle z|_{i+1,j,k+1} + 2\triangle z|_{i+1,j,k} + \triangle z|_{i+1,j,k-1}}.
\end{aligned}
\tag{5}
$$

The partial derivatives of the hydraulic head in the other five interfaces can be given by a similar expression. Substituting equation (5) into (4), multiplying both sides by $\Delta x|_{i,j,k}\Delta y|_{i,j,k}\Delta z|_{i,j,k}$, and rearranging terms, the following nineteen-point scheme results,

$$
\begin{aligned}
&Ah_{i,j+1,k} + Bh_{i,j,k} + Ch_{i+1,j+1,k} + Dh_{i-1,j+1,k} + Eh_{i+1,j,k} + Fh_{i-1,j,k} + \\
&Gh_{i,j+1,k+1} + Hh_{i,j+1,k-1} + Ih_{i,j,k+1} + Jh_{i,j,k-1} + Kh_{i,j-1,k} + Lh_{i+1,j-1,k} + \\
&Mh_{i-1,j-1,k} + Nh_{i,j-1,k+1} + Oh_{i,j-1,k-1} + Ph_{i+1,j,k+1} + Qh_{i+1,j,k-1} + \\
&Rh_{i-1,j,k+1} + Sh_{i-1,j,k-1} = -q_{i,j,k}\Delta x|_{i,j,k}\Delta y|_{i,j,k}\Delta z|_{i,j,k}.
\end{aligned}
\tag{6}
$$

where A$\sim$S can be determined by the block size and interface hydraulic conductivity components. Appendix A lists the specific expressions of A$\sim$S used in the code.

Two types of boundary conditions are taken into consideration in the process of building the system of linear equations: (1) Dirichlet condition that is utilized to model the interaction with the outside of the model domain and which is modeled by prescribing the head on the boundary, (2) Neuman condition that is used to model fixed source terms, in which the groundwater flux is specified (e.g., wells). Furthermore, a no-flow boundary, a special case of Neumann condition, is also considered.

The implementation of the two types of boundary conditions is as follows: (i) for prescribed heads we take advantage that we use an iterative approach for the solution of the linear system of equations, the prescribed head values at the corresponding blocks are set to their values at the beginning of the iterations and never updated during successive iterations, (ii) for prescribed fluxes through the boundaries, their values are assimilated inside the volumetric source vector q, whereas to handle no flow boundary conditions we always surround the entire domain with a skin of one block of inactive cells, in this way, equation (6) can be applied for all the active blocks without having to consider special cases for the blocks at the edges of the aquifer; then, for all inactive cells, the interface conductivity with adjacent blocks is set to zero, and, in addition, in order to compute the piezometric head gradient parallel to the interfaces a fictitious head value is assigned to these inactive cells equal to the average of the heads in the neighboring active blocks.

Also, when a well straddles several cells, the interface conductivities "inside" the well are set to a very large value and the pumping rate assigned to the bottommost cell.

With the above considerations for the boundary conditions, equation (6) is written for all active blocks within the aquifer, resulting in a system of linear equations that is solved using an iterative method based on a successive over relaxation (SOR) scheme.

Before the benchmarking of the proposed code and the LVDA package of MODFLOW (Harbaugh et al., 2000), it was verified in several synthetic exercises with scalar conductivities and various scenarios against MODFLOW, with results in perfect agreement. In fact, the nineteen-point finite-difference scheme proposed has no advantage with respect to MODFLOW or any other standard finite-difference simulator when the fluxes across numerical block interfaces induced by a hydraulic head gradient parallel to the interface are negligible. The proposed scheme is only of interest when these fluxes are important, that is, when the off-diagonal components of the hydraulic conductivity tensor controlling the flux across the interface are significant.

3. Program Description

The program takes as input values the hydraulic conductivity tensors at the block interfaces, these values must be provided by the user. In our experiments, we assume that they have been obtained by upscaling a fine scale conductivity field using the Laplacian with skin method (Gómez-Hernández, 1991) by means of the code described in the accompanying paper by Zhou et al. (2010).

The verification of the code will be carried out by comparing the specific discharges at the block interfaces with those resulting from the solution of the groundwater flow equation at the fine scale. Short of analytical expressions against which to compare our code results, the use of a fine scale simulation is a good alternative.

The different steps are the following:

1. Read initial interblock hydraulic conductivity tensors. These data can be derived by upscaling a fine scale simulation (Wen and Gómez-Hernández, 1996), generated using geostatistical methods (Deutsch and Journel, 1992), or simply by processing (averaging) the hydraulic conductivities at block centers, if they are available.
2. Read boundary condition data. As is the case for other forward simulators (e.g., MODFLOW), a boundary condition flag is stored in variable *ibound* with the following meaning:

$$\begin{aligned} &ibound(k,i,j) < 0; \quad \text{block } (k,i,j) \text{ has a prescribed head,} \\ &ibound(k,i,j) = 0; \quad \text{block } (k,i,j) \text{ is inactive,} \\ &ibound(k,i,j) > 0; \quad \text{block } (k,i,j) \text{ is active.} \end{aligned}$$

3. Read the initial guess heads to start the iterations. These initial heads must be equal to the prescribed head values at the blocks with prescribed head boundary conditions.
4. Set the interface conductivities to zero at impermeable boundaries and compute the fictitious head values at inactive cells (recall that these values are needed to compute the gradients parallel to the block interface)
5. Configure the linear system of equations by determining the nineteen coefficients in equation (6) for each active cell.
6. Solve the flow equation using an implicit technique (SOR). On each iteration, the heads at all active nodes are updated. Then, an intermediate value $\hat{h}_{k,i,j}$ is computed using the most recently updated values.

$$\begin{aligned} \hat{h}_{k,i,j} = \frac{1}{B}(&- Ah_{i,j+1,k} - Ch_{i+1,j+1,k} - Dh_{i-1,j+1,k} + Eh_{i+1,j,k} - Fh_{i-1,j,k} \\ &- Gh_{i,j+1,k+1} - Hh_{i,j+1,k-1} - Ih_{i,j,k+1} - Jh_{i,j,k-1} - Kh_{i,j-1,k} \\ &- Lh_{i+1,j-1,k} - Mh_{i-1,j-1,k} - Nh_{i,j-1,k+1} - Oh_{i,j-1,k-1} \\ &- Ph_{i+1,j,k+1} - Qh_{i+1,j,k-1} - Rh_{i-1,j,k+1} - Sh_{i-1,j,k-1} - q_{i,j,k}). \end{aligned} \tag{7}$$

   The updated head value for iteration $m+1$ is finally given by,

$$h^{m+1}_{k,i,j} = h^{m}_{k,i,j} + \omega(\hat{h}_{k,i,j} - h^{m}_{k,i,j}) \tag{8}$$

   where ω is the relaxation coefficient. When $\omega = 1$ the iterative scheme is the standard Gauss-Seidel algorithm. Iterations are stopped when the maximum absolute head change over all aquifer nodes is smaller than a predefined closure value.

   The above approach is not applied to prescribed head blocks, for which their value is not modified through the iterations. Once an iteration is completed, the fictitious heads at inactive cells are also updated by assigning to them the average value of the neighboring active blocks.
7. Once the head solution converges, Darcy's law is used to determine specific discharges $\mathbf{q}$ at block interfaces by,

$$\mathbf{q} = -\mathbf{K}\nabla h \tag{9}$$

The use of interblock conductivities as input parameters may seem not adequate as model input since, from an experimentalist point of view we regard conductivity as a material property associated to a certain aquifer volume. However, from an engineering point of view, we know that if the groundwater flow equation is to be solved by finite differences there is a need to approximate the hydraulic conductivity at the block interfaces. The choice is then to let the computer code to use some type of approximation to obtain this hydraulic conductivity or to try to get the best estimate for the interblock conductivity and feed it to the numerical solver.

This code originated as a tool to improve our methods for hydraulic conductivity upscaling (Zhou et al., 2010). In the upscaling process we can choose the volume for which we will compute the block hydraulic conductivity tensor and we found that it was much more precise to aim directly at computing the interblock conductivity rather than computing block centered conductivity tensors and let the code do the interblock approximation. We think that this situation may happen in contexts different from upscaling, and for this reason we wish to disseminate our code.

The source code, programmed in C++, and companion test examples are available to the public on the *IAMG* (*International Association for Mathematical Geosciences*) website. Appendix B provides an example of parameter file, and Appendix C explains input/output files in detail.

4. Synthetic Examples

This section demonstrates the algorithm presented in the previous section for two 2D heterogeneous realizations with uniform discretization, and a 3D example with nonuniform blocks.

All examples deal with heterogeneous fields, for which no analytical solution is available. For this reason, and in order to verify the accuracy of the solution, we always consider that the coarse model is the result of the upscaling of a fine scale model, with a higher resolution, characterized by scalar conductivities. On this fine-scale model, standard finite-difference numerical simulators can be used to compute heads and specific discharges that serve as the yardstick against which to measure the accuracy of the coarse scale simulations.

In all examples we proceed as follows: (i) we compute the hydraulic heads and the intercell fluxes at the fine scale using a standard finite-difference groundwater flow simulator, in this case we used MODFLOW, at this scale hydraulic conductivities are scalar and they are defined for each cell, (ii) from this fine scale simulation we determine the fluxes that should be reproduced at the coarse scale by integrating the fluxes along the coarse scale block sides, (iii) using the upscaling code by Zhou et al. (2010) we compute block centered hydraulic conductivity tensors to be used by MODFLOW-LVDA (only 2D examples), and interblock centered hydraulic conductivity tensors to be used by our code, (iv) we solve the flow equation at the coarse scale using MODFLOW-LVDA (only 2D examples) and our code, (v) and finally we compare the coarse scale fluxes to those obtained from the fine scale simulation in step (ii).

The reader should not be confused by the two meanings of the term anisotropy used in this paper: we refer to both spatial anisotropy and hydraulic anisotropy. At the fine scale we consider hydraulic conductivity as a scalar field with a spatial continuity characterized by a variogram function. The variogram is anisotropic indicating that there is preferential direction for the arrangement of the hydraulic conductivities (as is clearly noticeable in Figure 2). Thus there is no contradiction when we say, at the fine scale, that hydraulic conductivities are isotropic to flow, but spatially anisotropic. At the coarse scale, blocks of neighboring hydraulic conductivity cells are replaced by a single equivalent value; the spatial arrangement of the hydraulic conductivities within the block (characterized by the variogram function) may induce a hydraulic anisotropy to the block value, i.e., hydraulic head gradient and specific discharge vectors (at the coarse scale) do not have to be necessarily parallel. It should also be noticed that an isotropic spatial continuity at the fine scale conductivities does not warrant a scalar representation of the block value at the coarse scale.

4.1. Two Dimensional Examples

The hydraulic conductivity tensors at the interfaces are derived after upscaling two different fine scale fields that have been generated with different random function models. The fields at the fine scale are discretized with a mesh of 10 m by 10 m and extend on a square of 3000 m by 3000 m. We will refer to them

as models A and B. The ln$K$ field associated with model A was generated by Sequential Gaussian Simulation (GCOSIM3D) (Gómez-Hernández and Journel, 1993) with mean zero and unit variance, displaying a strong anisotropic spatial correlation in the 45° direction (see Figure 2). The correlation length in the largest continuity direction (x') is $\lambda_{x'} = 150$ m and in the smallest continuity direction (y') is $\lambda_{y'} = 30$ m. The variogram is exponential:

$$\gamma(\mathbf{r}) = 1.0 \cdot \left\{ 1 - \exp\left[- \sqrt{\left(\frac{3r_{x'}}{150}\right)^2 + \left(\frac{3r_{y'}}{30}\right)^2} \right] \right\} \tag{10}$$

with $\mathbf{r} = (r_{x'}, r_{y'})$ being the separation vector and

$$\begin{bmatrix} x' \\ y' \end{bmatrix} = \begin{bmatrix} 1/\sqrt{2} & 1/\sqrt{2} \\ -1/\sqrt{2} & 1/\sqrt{2} \end{bmatrix} \begin{bmatrix} x \\ y \end{bmatrix}. \tag{11}$$

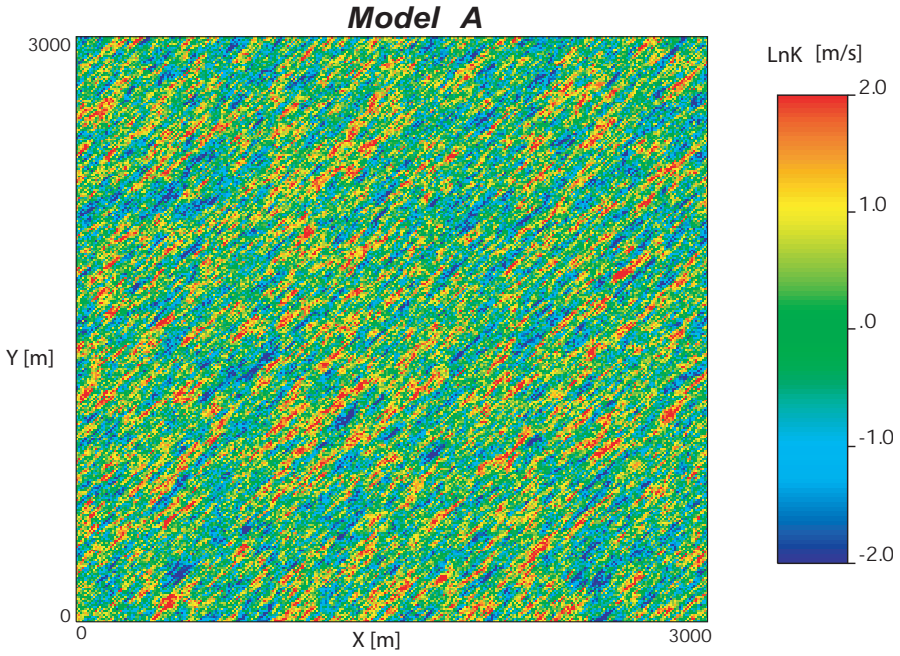

Figure 2: The fine scale hydraulic conductivity field used in model A. It was generated using Sequential Gaussian Simulation

We realize that for the simulation of groundwater flow for model A it would have been more convenient to align the Cartesian axes with the directions of maximum and minimum continuity of the hydraulic conductivities. However we wish to demonstrate that in those cases in which the fluxes across the interfaces are determined not only by the hydraulic head gradient orthogonal to it, but also by the head gradient parallel to the interface, it is very important to consider a value as accurate as possible for the interblock conductivity tensor. It is also true that, in many practical situations, the directions of the principal components of the hydraulic conductivity are not the uniform within the aquifer and therefore it is impossible to align the Cartesian axes with the hydraulic conductivity principal directions for all blocks, i.e., an aquifer on fluvial deposits, or a cross-bedded formation. We have chosen a limiting case in which the principal directions of the hydraulic conductivities at the coarse scale are as misaligned as possible with the Cartesian axes to demonstrate the importance of accounting for the full hydraulic conductivity tensor in those cases in which it is impossible to align axes and principal directions.

The fine scale hydraulic conductivity field associated with model B represents a sand/shale aquifer. The sand logconductivity values are generated by GCOSIM3D with zero mean and an isotropic exponential

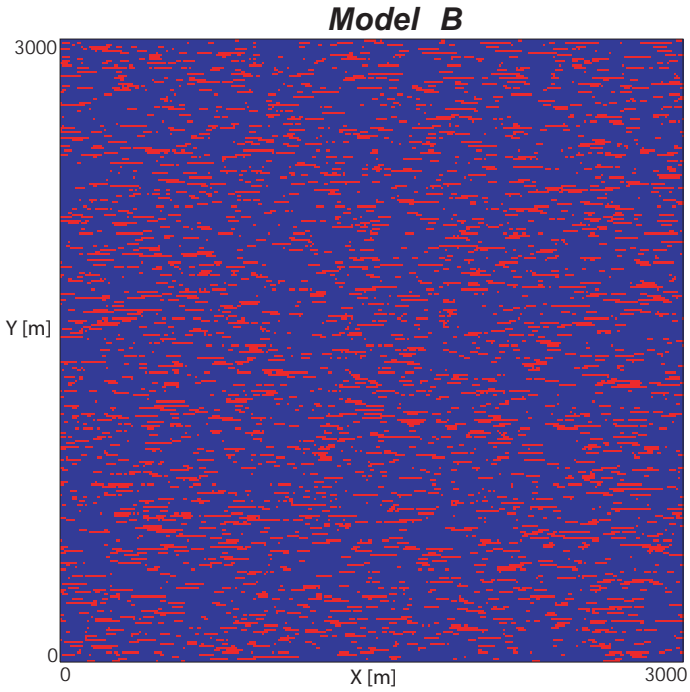

Figure 3: The fine scale hydraulic conductivity field used in model B. It was generated using Sequential Indicator Simulation (shales in red with $\ln K = -9$, sands in purple with mean $\ln K = 0$ and variance $\ln K = 1$, K units are m/s)

variogram function given by $\gamma(r) = 1 - \exp(-3r/\lambda)$, where the correlation length λ is set to 30 m. All shales are assigned a constant log-conductivity of -9 m/s. The distribution of sand and shales is generated by Sequential Indicator Simulation (ISIM3D) (Gómez-Hernández and Srivastava, 1990) using an indicator random function. The binary random function is defined as,

$$I(x) = \begin{cases} 1, & \text{if } x \text{ in shale} \\ 0, & \text{if } x \text{ in sand,} \end{cases} \tag{12}$$

with a mean value of $p = 0.15$, (15% of the aquifer is shale); variance of $p(1-p) = 0.1275$, and an exponential covariance function with correlation length in x direction $\lambda_x = 8$ m and negligible correlation in the y direction (Figure 3).

$$\gamma_I(r) = 0.1275\big[1 - \exp(-3|r_x|/\lambda_x)\big] \tag{13}$$

Both hydraulic conductivities fields are upscaled onto a coarser model. The coarse model extends over the inner 2400 m by 2400 m of the fine scale simulations with a discretization of 100 m by 100 m. The need to use a skin in the upscaling process (Gómez-Hernández, 1991) requires that the fine scale model extends beyond the limits of the coarse model. For the details on the upscaling process and how the interblock conductivities are computed, the reader is referred to the work by Zhou et al. (2010). For both model A and B, the skin used in the upscaling process is half the block size, i.e., 50 m, or 5 fine scale cells.

4.2. Flow Simulation

A forced-gradient flow problem is posed for both models over the 2400 m by 2400 m inner area of the fine scale realizations (see Figure 4). Prescribed heads are assigned on the perimeter of the model so that the average head gradient is parallel to the 45° direction. No sinks or sources are included.

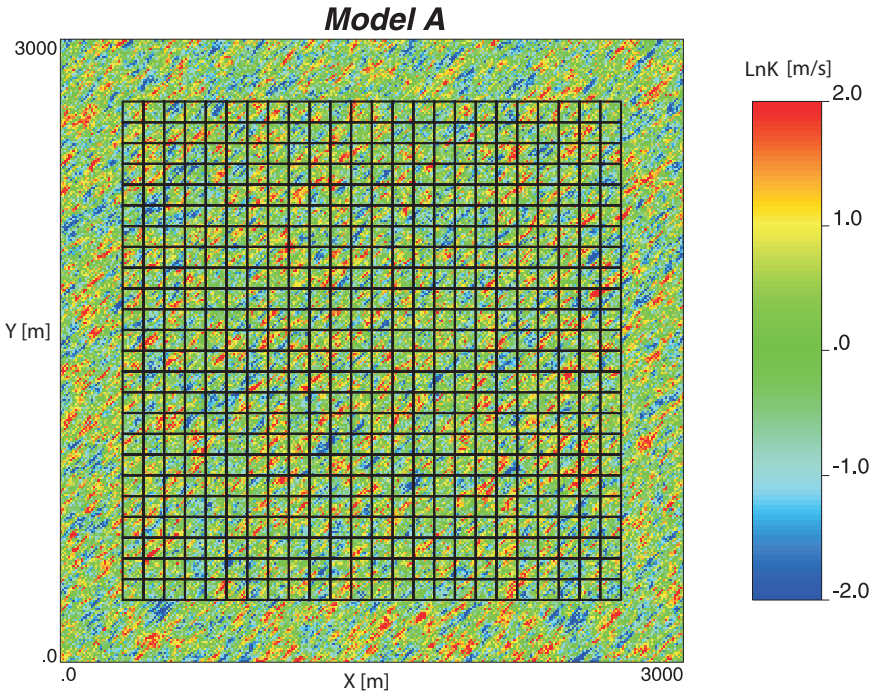

Figure 4: Model A fine scale hydraulic conductivity model overlaid with the discretization of the numerical model at the coarse scale

Flow is solved on the fine scale model over the 2400 m by 2400 m area, and the fluxes crossing the interfaces at the coarse scale discretization are computed. We will compare them to the flows obtained on the coarse scale model.

We compare the effectiveness of our approach with that of MODFLOW. For this purpose we focus on the reproduction of the fluxes at the block interfaces. We compare the coarse scale flows, that is, those obtained after solving the flow equation with the upscaled conductivities, with the reference flows, that is, those obtained from the solution of the flow equation at the fine scale. The mismatch between these two values is measured with the Relative Bias defined as,

$$RB = \left(\frac{1}{N} \sum_{N} \frac{|q_f - q_c|}{q_f} \right) \cdot 100, \tag{14}$$

where N is the number of blocks/interblocks used to compute the relative bias; q_f are the specific discharges computed on the fine scale solution, and q_c are the specific discharges from the coarse scale simulation.

Notice that we have chosen to analyze the goodness of the models by comparing the reproduction of the specific discharges, since these are much more sensitive than the hydraulic heads. Indeed, Figure 5 shows the hydraulic heads from the fine scale solution, and from the coarse scale solutions, calculated with the MODFLOW LVDA module and with the proposed simulator in model A. The differences in hydraulic heads are negligible; however, the discrepancy on the specific discharges is larger as will be shown later (see Figure 6). Recall that proper reproduction of the specific discharges is important in solute transport predictions.

In order to avoid the problems associated with the upscaling of the boundary conditions described by Vermeulen et al. (2006), only the inner 20 by 20 blocks are used to compute the relative bias. Figures 6 and 7 show the cross-plots between the specific discharges computed on the fine scale (reference values) and the ones computed on the coarse scale using the LVDA package from MODFLOW and the proposed approach. In the MODFLOW case, the upscaling code by Zhou et al. (2010) is used to compute the block conductivity

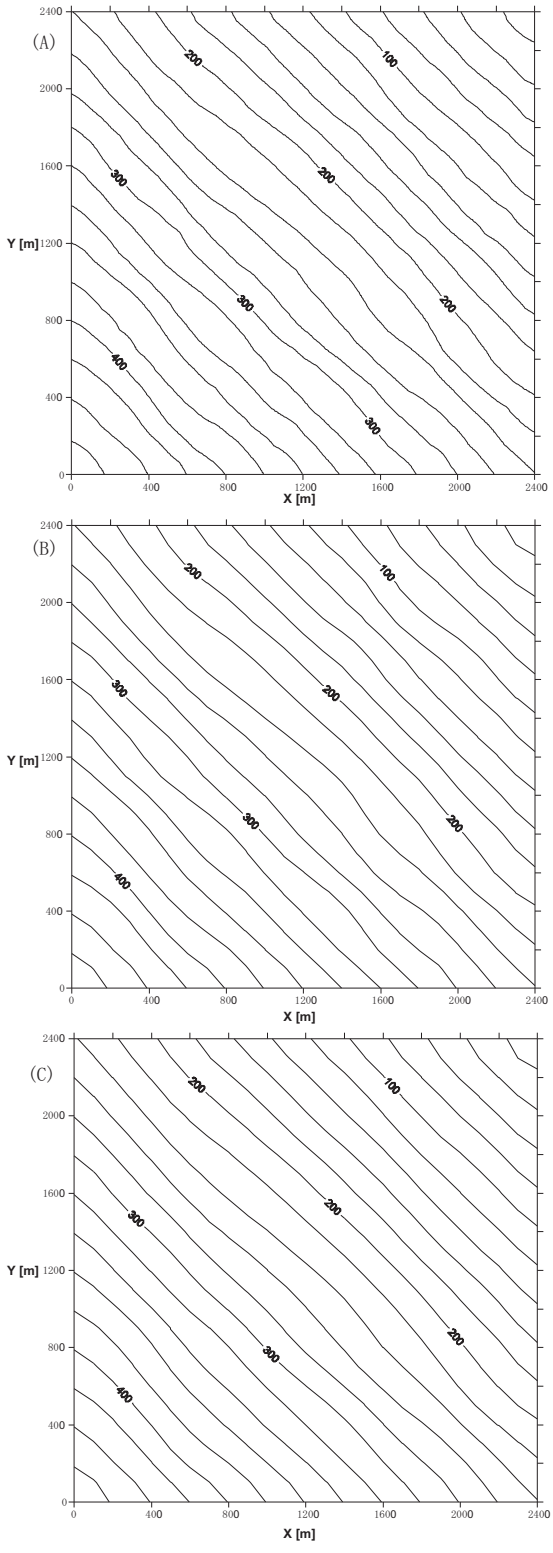

Figure 5: Contour lines of piezometric head for model A. (A) Contour lines obtained after within block averaging of the fine scale simulated heads. (B) Contour lines of the coarse heads obtained with the proposed simulator. (C), Contour lines of the coarse head obtained with MODFLOW using the LVDA package

.

tensors (instead of the tensors at the interfaces) since these are the parameters needed by the package. The LVDA package uses these block tensor values to approximate the conductivity tensors at the interfaces. It is clear that our numerical model outperforms MODFLOW LVDA package in both cases: for model A with the spatially anisotropic realization and for model B with the realization of sands and shales. The main reason for these results is the direct use of the interblock conductivities in our code, thus avoiding any averaging of block values to get to the interblock tensors.

The reader is referred to the full detailed explanation of the LVDA algorithm (Anderman et al., 2002). The LVDA package implemented in MODFLOW also uses a nine-point finite difference approximation (in 2D) to compute the fluxes across interfaces and to establish the volume balance equation. In MODFLOW, full transmissivity tensors are piecewise constant within each block. Since it is not trivial how to average transmissivity tensors of adjacent blocks to yield the interblock transmissivity value needed in equation (4), they resort to an internal refinement of the piezometric head grid using standard triangular basis functions to interpolate them at the midpoint of the interblock faces. With this new grid of piezometric heads and assuming a homogeneous piezometric head gradient within the block, MODFLOW-LVDA package proceeds to compute the fluxes crossing the interface from both sides of the interface, accounting for the flux induced by the piezometric head gradient orthogonal to the interface and also by the piezometric head gradient parallel to the interface. Continuity implies that these two values must be equal.

4.3. Application in Three Dimensions

In this subsection, we present an application of the code to a three dimensional example with a spatial anisotropy which is not parallel to any of the Cartesian axes. This case cannot be handled by the MODFLOW LVDA module, which only considers within-layer anisotropy. At the same time, we will check the code on a nonuniform discretization.

As in the 2D examples, we start with a fine scale realization, in this case generated over a grid of $120 \times 170 \times 70$ cells, each cell being a cube of 1 m by 1 m by 1 m (see Figure 8). The realization is generated by GCOSIM3D with a $\ln K$ distribution $\sim N(0, 1)$ and an isotropic exponential variogram with a correlation length of 20 m. The fine scale realization is upscaled onto a coarse model with 13 by 18 by 7 blocks of variable dimensions as shown in Figure 9 using the upscaling code by Zhou et al. (2010).

Note that the fact that the spatial variability of hydraulic conductivity is isotropic does not warrant that the interblock conductivity tensors are diagonal, thus the needed of using full tensor hydraulic conductivities at the interfaces.

The aquifer is confined and subject to linearly varying prescribed heads in the outside boundary that induce an overall head gradient oriented from the upper left corner in the top layer to the lower right corner in the bottom layer (Figure 9).

Figures 10 to 12 show the cross-plots for the specific discharges across the block faces in the coarse model against the specific discharges across the same block faces derived from the fine scale model. We have discriminated the fluxes according to the face orientation. We can see that the relative bias is small in all three orientations and that the reproduction of the specific discharges on the block faces of the coarse model approximate very well their values as derived from the detailed fine scale simulation. We can conclude that the proposed flow simulator is robust and accurate for the simulation of steady-state groundwater flow in three dimensions using full tensor hydraulic conductivities at the interblocks.

5. Conclusion

Modeling groundwater flow in anisotropic highly heterogeneous media calls for models capable to handle a tensorial description of hydraulic conductivity without the need of forcing all blocks to have the same principal directions, or that the principal directions be aligned in a specific orientation. Careful modeling of the hydraulic conductivities will yield accurate computation of aquifer fluxes, which are especially important for solute transport predictions. We have presented an algorithm and code that is capable to handle this generic description of the hydraulic conductivity tensor field and we have demonstrated its accuracy both in 2D and 3D, and also using uniform and nonuniform discretizations. The main characteristic of this code

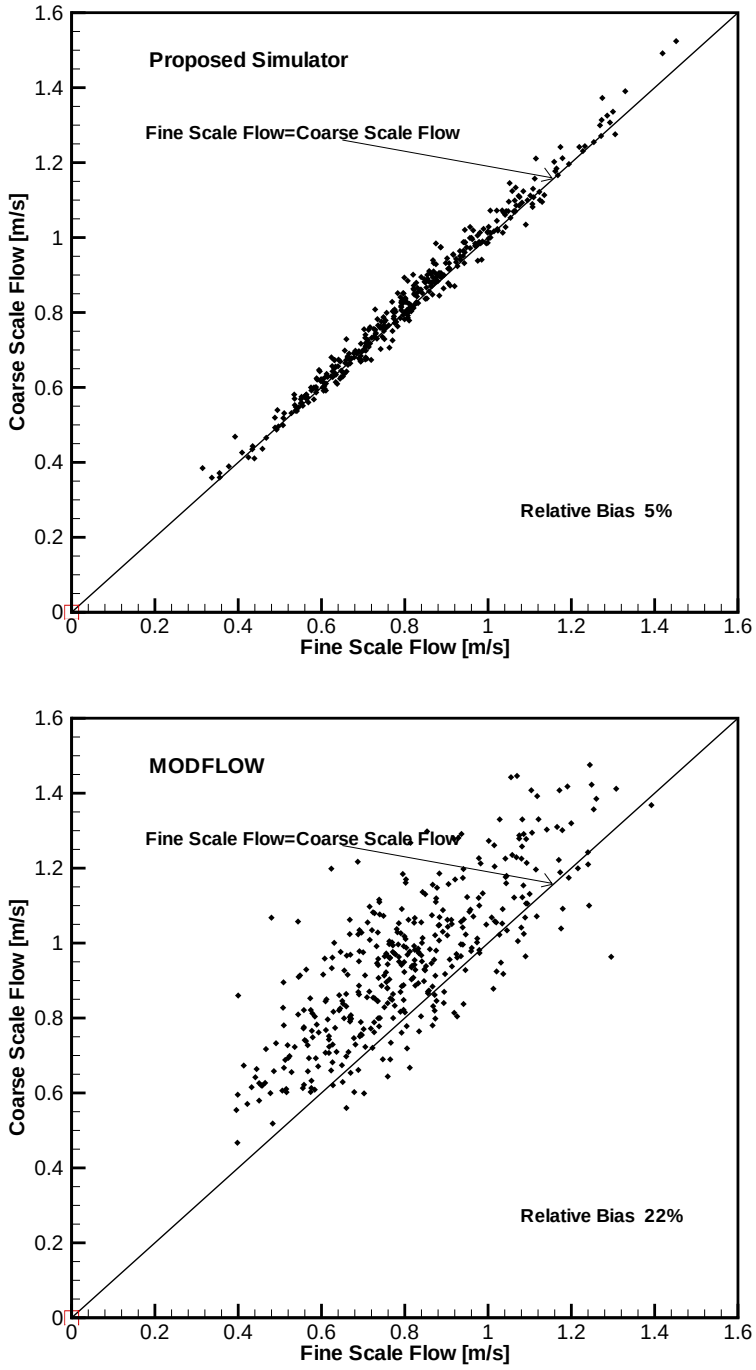

Figure 6: Flow comparison between the proposed simulator and MODFLOW in Model A.

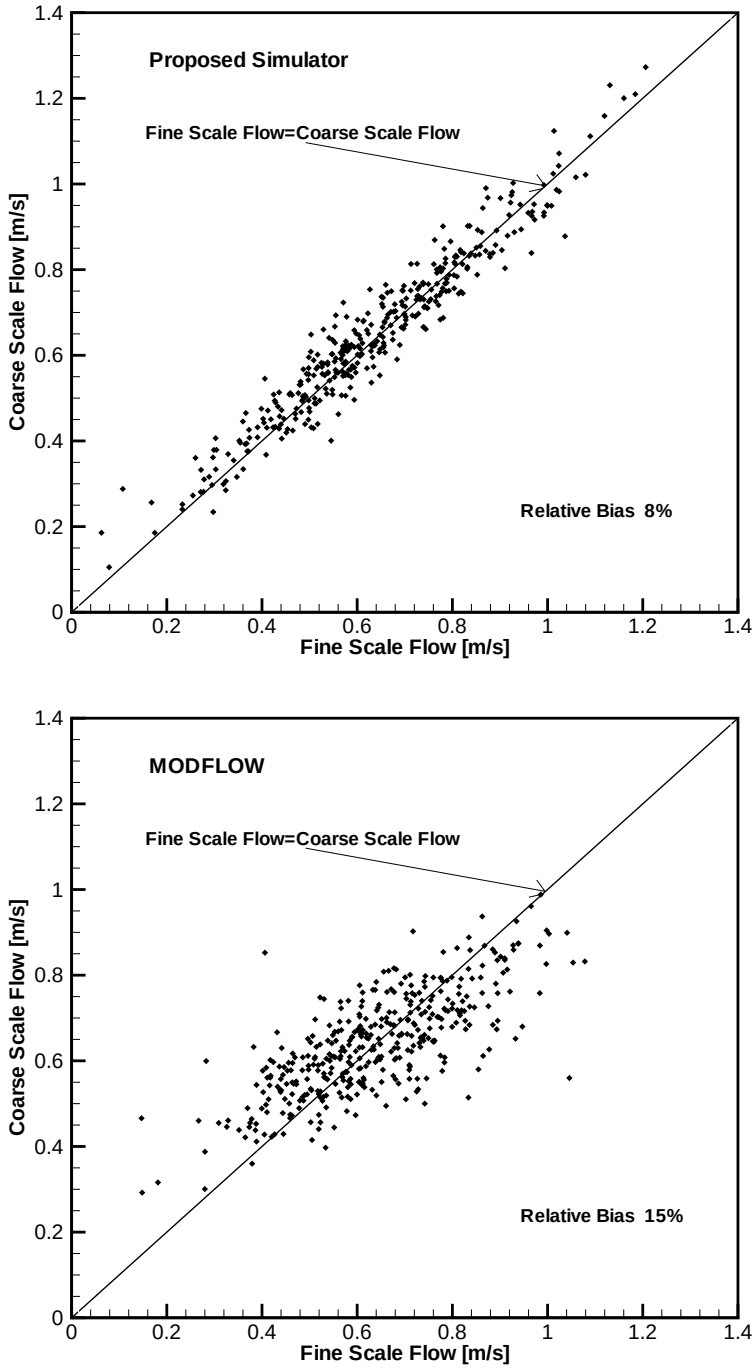

Figure 7: Flow comparison between the proposed simulator and MODFLOW in Model B.

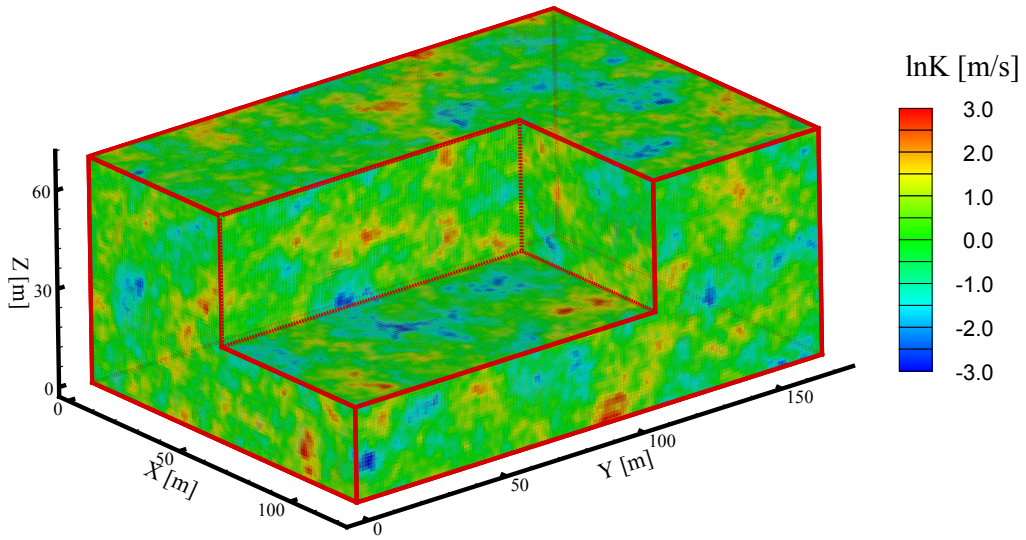

Figure 8: Reference ln$K$ field in three dimensions

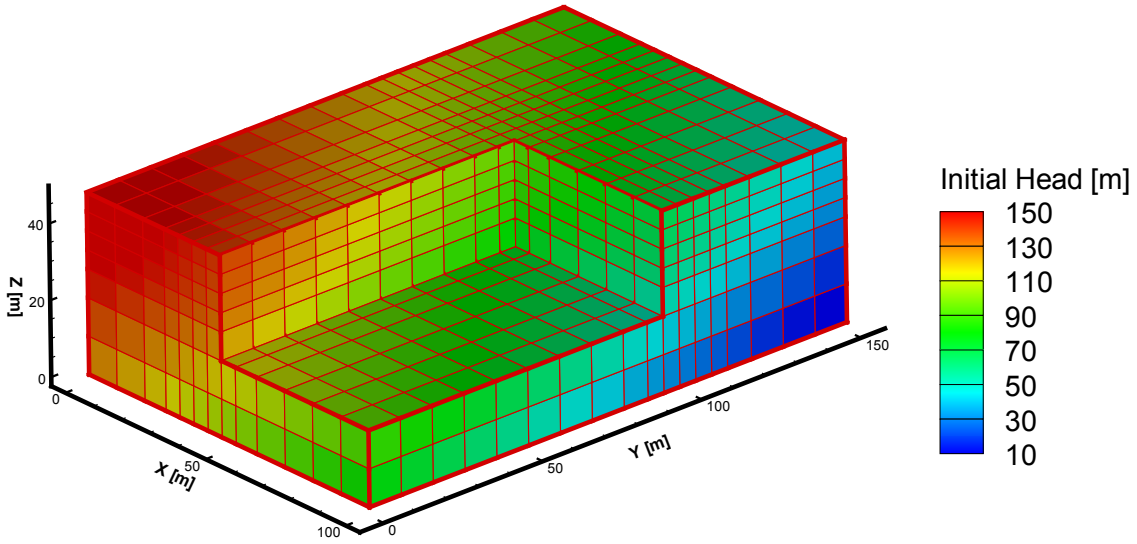

Figure 9: Nonuniform block discretization in three dimensions displaying the initial guess head values to start the iterations along with the prescribed heads at the boundaries

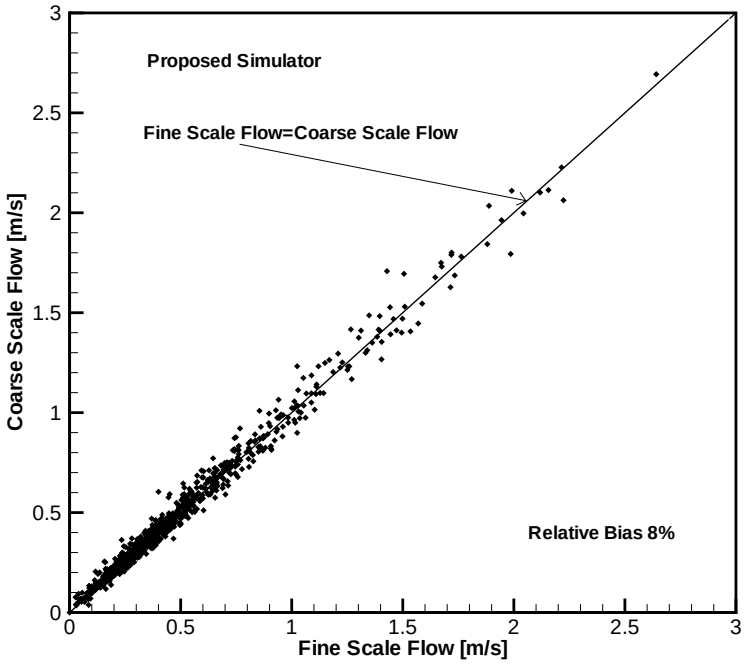

Figure 10: Flow comparison in X direction

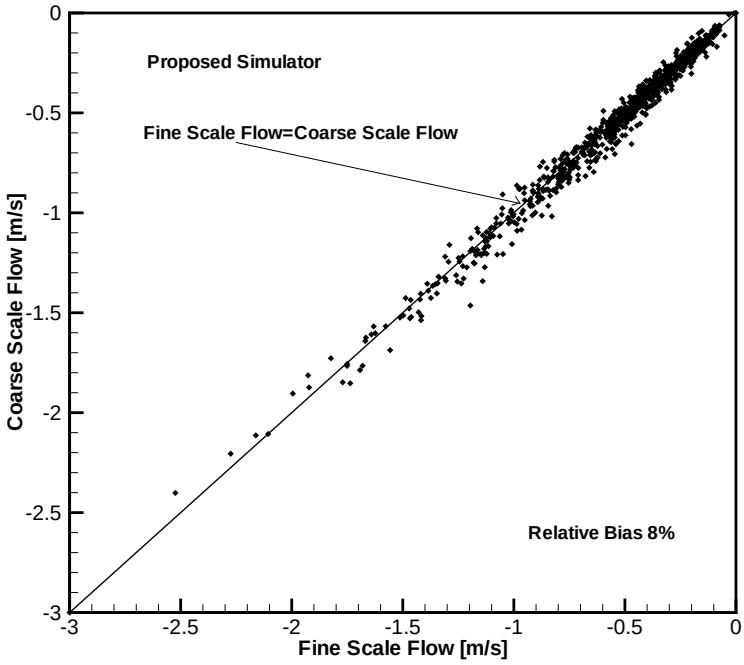

Figure 11: Flow comparison in Y direction

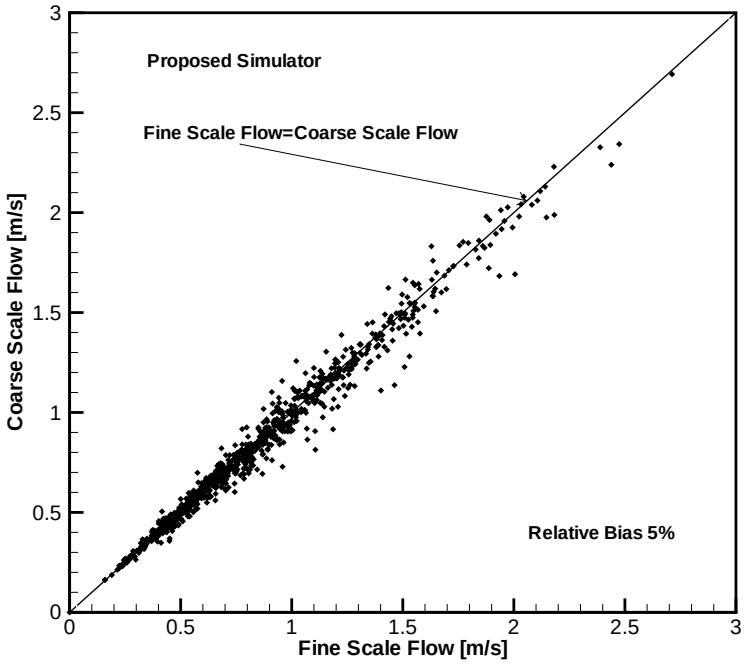

Figure 12: Flow comparison in Z direction

is that it works directly with the interblock tensor conductivities needed in the finite-difference formulation of the groundwater flow equation, thus avoiding unnecessary averaging of conductivities from neighboring blocks. This feature is the responsible for the better performance of our algorithm than the LVDA package in MODFLOW.

Although the examples presented are associated with the solution of an upscaling problem, the code is generic and could be used in any other context. The next step in the development of the code will be to incorporate transient capabilities.

Acknowledgements The authors gratefully acknowledge the financial support by ENRESA (project 0078000067) and the European Commission (projects FUNMIG and PAMINA). The second author also acknowledges the financial support by China Scholarship Council (CSC).

Appendix A: The expressions of A∼S used in the Equation (6)

$$
\begin{aligned}
A =& \triangle y|_{i,j,k}\triangle z|_{i,j,k}\left[\frac{2K_{xx}\big|_{i,j+1/2,k}}{\triangle x|_{i,j+1,k}+\triangle x|_{i,j,k}}\right]+\\
& \triangle x|_{i,j,k}\triangle z|_{i,j,k}\left[\frac{K_{yx}\big|_{i+1/2,j,k}-K_{yx}\big|_{i-1/2,j,k}}{\triangle x|_{i,j+1,k}+2\triangle x|_{i,j,k}+\triangle x|_{i,j-1,k}}\right]+\\
& \triangle x|_{i,j,k}\triangle y|_{i,j,k}\left[\frac{K_{zx}\big|_{i,j,k+1/2}-K_{zx}\big|_{i,j,k-1/2}}{\triangle x|_{i,j+1,k}+2\triangle x|_{i,j,k}+\triangle x|_{i,j-1,k}}\right]\\
B =& \triangle y|_{i,j,k}\triangle z|_{i,j,k}\left[\frac{-2K_{xx}\big|_{i,j+1/2,k}}{\triangle x|_{i,j+1,k}+\triangle x|_{i,j,k}}+\frac{-2K_{xx}\big|_{i,j-1/2,k}}{\triangle x|_{i,j,k}+\triangle x|_{i,j-1,k}}\right]+\\
& \triangle x|_{i,j,k}\triangle z|_{i,j,k}\left[\frac{-2K_{yy}\big|_{i+1/2,j,k}}{\triangle y|_{i+1,j,k}+\triangle y|_{i,j,k}}+\frac{-2K_{yy}\big|_{i-1/2,j,k}}{\triangle y|_{i,j,k}+\triangle y|_{i-1,j,k}}\right]+\\
& \triangle x|_{i,j,k}\triangle y|_{i,j,k}\left[\frac{-2K_{zz}\big|_{i,j,k+1/2}}{\triangle z|_{i,j,k+1}+\triangle z|_{i,j,k}}+\frac{-2K_{zz}\big|_{i,j,k-1/2}}{\triangle z|_{i,j,k}+\triangle z|_{i,j,k-1}}\right]\\
C =& \triangle y|_{i,j,k}\triangle z|_{i,j,k}\left[\frac{K_{xy}\big|_{i,j+1/2,k}}{\triangle y|_{i+1,j+1,k}+2\triangle y|_{i-1,j+1,k}+\triangle y|_{i,j+1,k}}\right]+\\
& \triangle x|_{i,j,k}\triangle z|_{i,j,k}\left[\frac{K_{yx}\big|_{i+1/2,j,k}}{\triangle x|_{i+1,j+1,k}+2\triangle x|_{i+1,j-1,k}+\triangle x|_{i+1,j,k}}\right]\\
D =& \triangle y|_{i,j,k}\triangle z|_{i,j,k}\left[\frac{-K_{xy}\big|_{i,j+1/2,k}}{\triangle y|_{i+1,j+1,k}+2\triangle y|_{i-1,j+1,k}+\triangle y|_{i,j+1,k}}\right]+\\
& \triangle x|_{i,j,k}\triangle z|_{i,j,k}\left[\frac{-K_{yx}\big|_{i-1/2,j,k}}{\triangle x|_{i-1,j+1,k}+2\triangle x|_{i-1,j-1,k}+\triangle x|_{i-1,j,k}}\right]\\
E =& \triangle y|_{i,j,k}\triangle z|_{i,j,k}\left[\frac{K_{xy}\big|_{i,j+1/2,k}-K_{xy}\big|_{i,j-1/2,k}}{\triangle y|_{i+1,j,k}+2\triangle y|_{i,j,k}+\triangle y|_{i-1,j,k}}\right]+\\
& \triangle x|_{i,j,k}\triangle z|_{i,j,k}\left[\frac{2K_{yy}\big|_{i+1/2,j,k}}{\triangle y|_{i+1,j,k}+\triangle y|_{i,j,k}}\right]+\\
& \triangle x|_{i,j,k}\triangle y|_{i,j,k}\left[\frac{K_{zy}\big|_{i,j,k+1/2}-K_{zy}\big|_{i,j,k-1/2}}{\triangle y|_{i+1,j,k}+2\triangle y|_{i,j,k}+\triangle y|_{i-1,j,k}}\right]\\
F =& \triangle y|_{i,j,k}\triangle z|_{i,j,k}\left[\frac{K_{xy}\big|_{i,j-1/2,k}-K_{xy}\big|_{i,j+1/2,k}}{\triangle y|_{i+1,j,k}+2\triangle y|_{i,j,k}+\triangle y|_{i-1,j,k}}\right]+\\
& \triangle x|_{i,j,k}\triangle z|_{i,j,k}\left[\frac{2K_{yy}\big|_{i-1/2,j,k}}{\triangle y|_{i,j,k}+\triangle y|_{i-1,j,k}}\right]+\\
& \triangle x|_{i,j,k}\triangle y|_{i,j,k}\left[\frac{K_{zy}\big|_{i,j,k-1/2}-K_{zy}\big|_{i,j,k+1/2}}{\triangle y|_{i+1,j,k}+2\triangle y|_{i,j,k}+\triangle y|_{i-1,j,k}}\right]
\end{aligned}
$$

$$
\begin{aligned}
G =& \triangle y|_{i,j,k}\triangle z|_{i,j,k}\left[\frac{K_{xz}\big|_{i,j+1/2,k}}{\triangle z|_{i,j+1,k+1}+2\triangle z|_{i,j+1,k}+\triangle z|_{i,j+1,k-1}}\right]+\\
& \triangle x|_{i,j,k}\triangle y|_{i,j,k}\left[\frac{K_{zx}\big|_{i,j,k+1/2}}{\triangle x|_{i,j+1,k+1}+2\triangle x|_{i,j,k+1}+\triangle x|_{i,j-1,k+1}}\right]\\
H =& \triangle y|_{i,j,k}\triangle z|_{i,j,k}\left[\frac{-K_{xz}\big|_{i,j+1/2,k}}{\triangle z|_{i,j+1,k+1}+2\triangle z|_{i,j+1,k}+\triangle z|_{i,j+1,k-1}}\right]+\\
& \triangle x|_{i,j,k}\triangle y|_{i,j,k}\left[\frac{-K_{zx}\big|_{i,j,k-1/2}}{\triangle x|_{i,j+1,k-1}+2\triangle x|_{i,j,k-1}+\triangle x|_{i,j-1,k-1}}\right]\\
I =& \triangle y|_{i,j,k}\triangle z|_{i,j,k}\left[\frac{K_{xz}\big|_{i,j+1/2,k}-K_{xz}\big|_{i,j-1/2,k}}{\triangle z|_{i,j,k+1}+2\triangle z|_{i,j,k}+\triangle z|_{i,j,k-1}}\right]+\\
& \triangle x|_{i,j,k}\triangle z|_{i,j,k}\left[\frac{K_{yz}\big|_{i+1/2,j,k}-K_{yz}\big|_{i-1/2,j,k}}{\triangle z|_{i,j,k+1}+2\triangle z|_{i,j,k}+\triangle z|_{i,j,k-1}}\right]+\\
& \triangle x|_{i,j,k}\triangle y|_{i,j,k}\left[\frac{2K_{zz}\big|_{i,j,k+1/2}}{\triangle z|_{i,j,k+1}+\triangle z|_{i,j,k}}\right]\\
J =& \triangle y|_{i,j,k}\triangle z|_{i,j,k}\left[\frac{K_{xz}\big|_{i,j-1/2,k}-K_{xz}\big|_{i,j+1/2,k}}{\triangle z|_{i,j,k+1}+2\triangle z|_{i,j,k}+\triangle z|_{i,j,k-1}}\right]+\\
& \triangle x|_{i,j,k}\triangle z|_{i,j,k}\left[\frac{K_{yz}\big|_{i-1/2,j,k}-K_{yz}\big|_{i+1/2,j,k}}{\triangle z|_{i,j,k+1}+2\triangle z|_{i,j,k}+\triangle z|_{i,j,k-1}}\right]+\\
& \triangle x|_{i,j,k}\triangle y|_{i,j,k}\left[\frac{2K_{zz}\big|_{i,j,k-1/2}}{\triangle z|_{i,j,k-1}+\triangle z|_{i,j,k}}\right]\\
K =& \triangle y|_{i,j,k}\triangle z|_{i,j,k}\left[\frac{2K_{xx}\big|_{i,j-1/2,k}}{\triangle x|_{i,j,k}+\triangle x|_{i,j-1,k}}\right]+\\
& \triangle x|_{i,j,k}\triangle z|_{i,j,k}\left[\frac{(K_{yx}\big|_{i-1/2,j,k}-K_{yx}\big|_{i+1/2,j,k})}{\triangle x|_{i,j+1,k}+2\triangle x|_{i,j,k}+\triangle x|_{i,j-1,k}}\right]+\\
& \triangle x|_{i,j,k}\triangle y|_{i,j,k}\left[\frac{(K_{zx}\big|_{i-1/2,j,k}-K_{zx}\big|_{i+1/2,j,k})}{\triangle x|_{i,j+1,k}+2\triangle x|_{i,j,k}+\triangle x|_{i,j-1,k}}\right]\\
L =& \triangle y|_{i,j,k}\triangle z|_{i,j,k}\left[\frac{-K_{xy}\big|_{i,j-1/2,k}}{\triangle y|_{i+1,j-1,k}+2\triangle y|_{i,j-1,k}+\triangle y|_{i-1,j-1,k}}\right]+\\
& \triangle x|_{i,j,k}\triangle z|_{i,j,k}\left[\frac{-K_{yx}\big|_{i+1/2,j,k}}{\triangle x|_{i+1,j+1,k}+2\triangle x|_{i+1,j-1,k}+\triangle x|_{i+1,j,k}}\right]\\
M =& \triangle y|_{i,j,k}\triangle z|_{i,j,k}\left[\frac{K_{xy}\big|_{i,j-1/2,k}}{\triangle y|_{i+1,j-1,k}+2\triangle y|_{i,j-1,k}+\triangle y|_{i-1,j-1,k}}\right]+\\
& \triangle x|_{i,j,k}\triangle z|_{i,j,k}\left[\frac{K_{yx}\big|_{i-1/2,j,k}}{\triangle x|_{i-1,j+1,k}+2\triangle x|_{i-1,j-1,k}+\triangle x|_{i-1,j,k}}\right]
\end{aligned}
$$

$$
\begin{aligned}
N =& \triangle y|_{i,j,k} \triangle z|_{i,j,k} \left[\frac{-K_{xz}\big|_{i,j-1/2,k}}{\triangle z|_{i,j-1,k+1} + 2\triangle z|_{i,j-1,k} + \triangle z|_{i,j-1,k-1}} \right] + \\
& \triangle x|_{i,j,k} \triangle y|_{i,j,k} \left[\frac{-K_{zx}\big|_{i,j,k+1/2}}{\triangle x|_{i,j+1,k+1} + 2\triangle x|_{i,j,k+1} + \triangle x|_{i,j-1,k+1}} \right] \\
O =& \triangle y|_{i,j,k} \triangle z|_{i,j,k} \left[\frac{K_{xz}\big|_{i,j-1/2,k}}{\triangle z|_{i,j-1,k+1} + 2\triangle z|_{i,j-1,k} + \triangle z|_{i,j-1,k-1}} \right] + \\
& \triangle x|_{i,j,k} \triangle y|_{i,j,k} \left[\frac{K_{zx}\big|_{i,j,k-1/2}}{\triangle x|_{i,j+1,k-1} + 2\triangle x|_{i,j,k-1} + \triangle x|_{i,j-1,k-1}} \right] \\
P =& \triangle y|_{i,j,k} \triangle z|_{i,j,k} \left[\frac{K_{yz}\big|_{i+1/2,j,k}}{\triangle z|_{i+1,j,k+1} + 2\triangle z|_{i+1,j,k} + \triangle z|_{i+1,j,k-1}} \right] + \\
& \triangle x|_{i,j,k} \triangle y|_{i,j,k} \left[\frac{K_{zy}\big|_{i,j,k+1/2}}{\triangle y|_{i+1,j,k+1} + 2\triangle y|_{i,j,k+1} + \triangle y|_{i-1,j,k+1}} \right] \\
Q =& \triangle y|_{i,j,k} \triangle z|_{i,j,k} \left[\frac{-K_{yz}\big|_{i+1/2,j,k}}{\triangle z|_{i+1,j,k+1} + 2\triangle z|_{i+1,j,k} + \triangle z|_{i+1,j,k-1}} \right] + \\
& \triangle x|_{i,j,k} \triangle y|_{i,j,k} \left[\frac{-K_{zy}\big|_{i,j,k-1/2}}{\triangle y|_{i+1,j,k-1} + 2\triangle y|_{i,j,k-1} + \triangle y|_{i-1,j,k-1}} \right] \\
R =& \triangle y|_{i,j,k} \triangle z|_{i,j,k} \left[\frac{-K_{yz}\big|_{i-1/2,j,k}}{\triangle z|_{i-1,j,k+1} + 2\triangle z|_{i-1,j,k} + \triangle z|_{i-1,j,k-1}} \right] + \\
& \triangle x|_{i,j,k} \triangle y|_{i,j,k} \left[\frac{-K_{zy}\big|_{i,j,k+1/2}}{\triangle y|_{i+1,j,k+1} + 2\triangle y|_{i,j,k+1} + \triangle y|_{i-1,j,k+1}} \right] \\
S =& \triangle y|_{i,j,k} \triangle z|_{i,j,k} \left[\frac{K_{yz}\big|_{i-1/2,j,k}}{\triangle z|_{i-1,j,k+1} + 2\triangle z|_{i-1,j,k} + \triangle z|_{i-1,j,k-1}} \right] + \\
& \triangle x|_{i,j,k} \triangle y|_{i,j,k} \left[\frac{K_{zy}\big|_{i,j,k-1/2}}{\triangle y|_{i+1,j,k-1} + 2\triangle y|_{i,j,k-1} + \triangle y|_{i-1,j,k-1}} \right].
\end{aligned}
$$

Appendix B: Example of Parameter File

```
*********************************************************
*                  Parameter File                       *
*       Technical University of Valencia,Spain          *
*              Liangping Li, Sep. 2009                  *
*    All input and output files have a GeoEAS format.   *
*********************************************************
13 18 7            ** ncol, nrow, nlay
1 1 1              ** flag of dx,dy,dz: 0(const);1(file)
10 10 10           ** constant dx, dy, dz if(0)
interval_x.dat     ** Filename of dx if(1)
interval_y.dat     ** Filename of dY if(1)
interval_z.dat     ** Filename of dZ if(1)
1  1e-7 10000      ** accel, closure(e-9), maxiter
kxx.txt            ** Filename of conductances between columns
```

```
kyy.txt            ** Filename of conductances between rows
kzz.txt            ** Filename of conductances between layers
ihead.dat          ** Filename of intial guess head
ibound.dat         ** Filename of boundary condition
Head.dat           ** Filename of simulated head
qx.dat             ** Filename of calculated flow in x direction
qy.dat             ** Filename of calculated flow in y direction
qz.dat             ** Filename of calculated flow in z direction
-------------well
0                  ** Number of well
well.txt           ** Filename of well information
-------------Debug
0                  ** debug yes(>=1),no(0)
-------------END----------------
```

Appendix C: Explanation of Input/Output Files

```
Flowxyz: A C program to simulate steady-state groundwater flow with
         full tensor hydraulic conductivities by finite-difference
         in three dimensions.

Compile this code with a C++ compiler (e.g., Microsoft Virsual C++
6.0).

Example input parameter file as well as input/output data are given,
where:

1) flowxyz.par   : parameter file
2) interval_x.dat: x direction cell size for nonuniform blocks [ncol]
3) interval_y.dat: y direction cell size for nonuniform blocks [nrow]
4) interval_z.dat: z direction cell size for nonuniform blocks [nlay]
5) kxx.dat       : the interface conductivity between columns
                   [(ncol-1)*nrow *nlay    ]
6) kyy.dat       : the interface conductivity between rows
                   [(ncol-1)*nrow *nlay    ]
7) kzz.dat       : the interface conductivity between layers
                   [ncol    *nrow *(nlay-1)]
8) ihead.dat     : the initial guess head         [ncol*nrow*nlay]
9) ibound.dat    : the initial boundary condition [ncol*nrow*nlay]
10) Head.dat     : the simulated head             [ncol*nrow*nlay]
11) qx.dat       : the calculated flow in the x direction
                   [(ncol-1)*nrow    *nlay    ]
12) qy.dat       : the calculated flow in the y direction
                   [ncol    *(nrow-1)*nlay    ]
13) qz.dat       : the calculated flow in the z direction
                   [ncol    *nrow    *(nlay-1)]
14) well.dat     : the well information [nrow,ncol,nlay,Q(L3T-1)]
```

References

Aavatsmark, I., Barkve, T., øBøe, Mannseth, T., 1996. Discretization on non-orthogonal, quadrilateral grids for inhomogeneous, anisotropic media. Journal of Computational Physics 127 (1), 2–14.

Anderman, E. R., Kipp, K. L., Hill, M. C., Valstar, J., Neupauer, R. M., 2002. MODFLOW-2000, the US geological survey modular Ground-Water Model Documentation of the Model-Layer Variable-Direction horizontal anisotropy (LVDA) capability of the Hydrogeologic-Unit flow (HUF) package. US Geological Survey, Open file Report, 02-409, 60pp.

Bear, J., 1972. Dynamics of fluids in porous media. American Elsevier Pub. Co., New York, 764pp.

Bierkens, M. F. P., Weerts, H. J. T., 1994. Block hydraulic conductivity of cross-bedded fluvial sediments. Water Resources Research 30 (10), 2665–2678.

Deutsch, C. V., Journel, A. G., 1992. GSLIB, Geostatistical Software Library and User's Guide. Oxford University Press, New York, 369pp.

Duvaut, G., Lions, J. L., John, C. W., 1976. Inequalities in mechanics and physics. Springer Verlag, 397pp.

Edwards, M. G., Rogers, C. F., 1998. Finite volume discretization with imposed flux continuity for the general tensor pressure equation. Computational Geosciences 2 (4), 259–290.

Gómez-Hernández, J. J., 1991. A stochastic approach to the simulation of block conductivity values conditioned upon data measured at a smaller scale. Ph.D. thesis, Stanford University, 351pp.

Gómez-Hernández, J. J., Journel, A. G., 1993. Joint sequential simulation of multi-Gaussian fields. Geostatistics Troia 92 (1), 85–94.

Gómez-Hernández, J. J., Srivastava, R. M., 1990. ISIM3D: an ANSI-C three dimensional multiple indicator conditional simulation program. Computers and Geosciences 16 (4), 395–440.

Harbaugh, A. W., Banta, E. R., Hill, M. C., McDonald, M. G., 2000. MODFLOW-2000, the U.S. Geological Survey modular ground-water model. U.S. Geological Survey, Branch of Information Services, Reston, VA, Denver, CO, 121pp.

Penman, J., 1988. Dual and complementary variational techniques for the calculation of electromagnetic fields. Advances in Electronics and Electron Physics. 70, 315–364.

Rehfeldt, K. R., Boggs, J. M., Gelhar, L. W., 1992. Field study of dispersion in a heterogeneous aquifer 3. geostatistical analysis of hydraulic conductivity. Water Resources Research 28 (12), 3309–3324.

Rozon, B., 1989. A generalized finite volume discretization method for reservoir simulation. SPE paper 18414.

Vermeulen, P. T. M., Stroet, C. B. M. T., Heemink, A. W., 2006. Limitations to upscaling of groundwater flow models dominated by surface water interaction. Water Resources Research 42 (10), W10406, doi:10.1029/2005WR004620.

Wen, X., Gómez-Hernández, J. J., 1996. Upscaling hydraulic conductivities: An overview. Journal of Hydrology 183 (1-2), ix–xxxii.

Zhou, H. Y., Li, L. P., Gómez-Hernández, J. J., 2010. Three-dimensional hydraulic conductivity upscaling in groundwater modelling. Computers and Geosciences Accepted.